Control Parameters for the Influence of a Mesoscale Mountain Range on Cyclone Track Continuity and Deflection

YUH-LANG LIN, SHU-YUN CHEN, AND CHRISTOPHER M. HILL

North Carolina State University, Raleigh, North Carolina

CHING-YUANG HUANG

National Central University, Chung-Li, Taiwan

(Manuscript received 13 April 2004, in final form 5 October 2004)

ABSTRACT

In this study prospective control parameters are identified for diagnosing the continuity and deflection of cyclone tracks across a mesoscale mountain range. Based on idealized simulations of a westward-moving cyclone, it was found that the cyclone track becomes a discontinuous (continuous) track and the cyclone experiences more (less) deflection with a combination of small (large) values of V_{max}/Nh, U/Nh, R/L_y, U/fL_x, and V_{max}/fR, and large (small) value of h/L_x. The symbols are defined as follows: V_{max} the maximum tangential wind, N the Brunt–Väisälä frequency, h the mountain height, U the basic wind speed, R the radius of V_{max}, f the Coriolis parameter, and L_x and L_y the horizontal scales of the mountain in x and y directions, respectively.

A conceptual model is proposed to explain track deflection and continuity for a westward-moving cyclone encountering idealized topography representative of the Central Mountain Range of Taiwan. With weak orographic blocking, a cyclone crosses over the mountain range with some northward deflection. With moderate orographic blocking, northward deflection of a cyclone is greater upstream of the mountain range and a secondary, leeside vortex forms to the southwest of the mountain range, indicative of discontinuity in the cyclone track. With strong orographic blocking, a westward-moving cyclone is deflected southward and a secondary cyclone forms to the northwest of the mountain range. The northward or southward deflection of a cyclone track is explained by the orographic blocking on the outer circulation of the cyclone.

1. Introduction

As a tropical cyclone (TC) passes over a mesoscale mountain range, the motion, strength, and coherence of its circulation core can be significantly perturbed by the topography. Such influence has been observed with the Central Mountain Range (CMR) of Taiwan, the Cordillera Central of Hispañola, and the Cordillera Central of northern Luzon in the Philippines (e.g., Wang 1980; Bender et al. 1987; Lin 1993). In particular, orographic influence on TC track continuity and deflection has been studied extensively over the CMR, a mountain range that lends favorably to research in terms of both geography and TC climatology. This steep, isolated mountain range is oriented north-northeast to south-southwest, is surrounded by significant bodies of water, and is on the path for many western Pacific TCs.

Wang (1980) found that the center of a TC crosses the CMR either continuously or discontinuously (Fig. 1; also see Lin et al. 1999, hereafter LHHH; Wu and Kuo 1999). Typhoons with a continuous track (Fig. 1a) tend to pass over the island in a cyclonically curved path. For typhoons with a discontinuous track (Fig. 1b), two or more secondary, low-level low pressure centers tend to form over the lee (west) side of the CMR as the parent cyclone approaches upstream of the mountain (Wang 1980). In this study, a cyclone track is defined as discontinuous when the original cyclone (i.e., a low pressure and closed cyclonic circulation) and a lee vortex simultaneously coexist; the track is traced by the maximum vorticity center. The leeside formation of low pressure centers corresponds with the approach of a typhoon with maximum tangential wind speed (V_{max}) in the range of 25–50 m s^{-1}, or with a cyclonic circulation depth (D) less than 6 km. One of the secondary low pressure centers can develop further and eventually replace the original, low-level cyclone low pressure center blocked to the east of the CMR. Conversely, a typhoon with a stronger ($V_{max} > 50$ m s^{-1}) or deeper ($D > 10.7$ km) circulation can be followed continuously, and the resulting track is, thus, continuous. Brand and Blelloch (1974) found that the maximum surface wind speed of

Corresponding author address: Dr. Yuh-Lang Lin, Department of Marine, Earth, and Atmospheric Sciences, North Carolina State University, Raleigh, NC 27695-8208.
E-mail: yl_lin@ncsu.edu

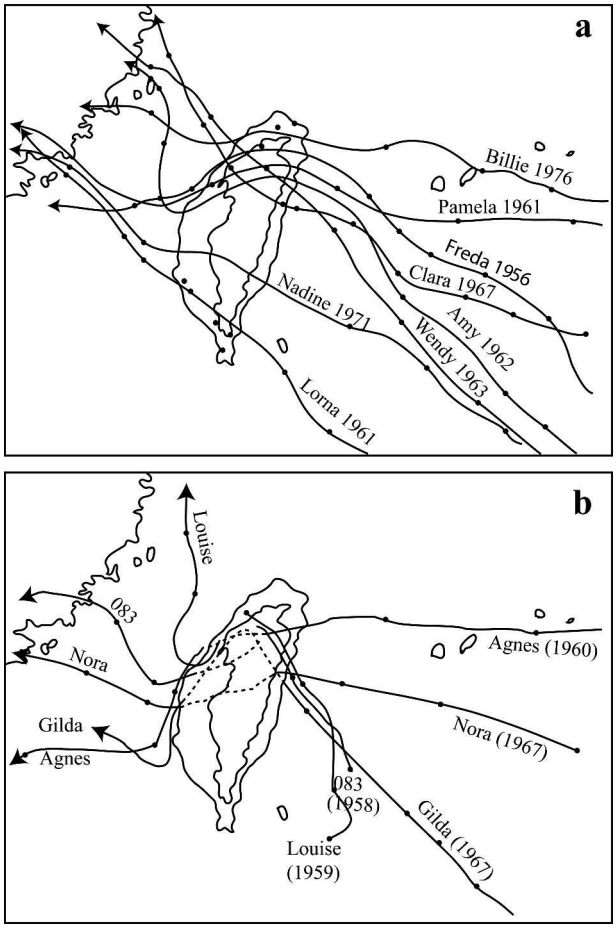

FIG. 1. Tropical cyclones traversing the Central Mountain Range of Taiwan with (a) continuous tracks and (b) discontinuous tracks. (Adapted after Wang 1980; Chang 1982; LHHH.)

a typhoon decreases by over 40% and a distinct northward deflection in the motion of a typhoon occurs as a typhoon approaches the CMR from the east or southeast. Therefore, continuity and deflection of a TC track may be controlled by V_{max} and D of the TC and, naturally, the mountain height (h).

Chang (1982) made the first attempt to conduct numerical simulations of westward-moving tropical cyclones over idealized CMR using a primitive equation model. He proposed that the cyclonically curved path of an approaching cyclone center is the result of influence from cumulus heating, horizontal vorticity advection, and of leeside vorticity stretching of the basic flow. One of the secondary vortex centers that form within a lee trough can develop further when in phase with the upper-level vortex. The numerical simulations by Chang (1982) are consistent with the observations of Wang (1980) and others. Based on numerical simulations, Bender et al. (1987) found that cyclone track deflection is sensitive to the basic flow speed and proposed that terrain-induced environmental flow is the main cause of track deflection. Therefore, in addition to V_{max}, D, and h, the basic flow speed (U) may also serve as a control parameter of TC track continuity and deflection.

In a combined observational and numerical modeling study, Yeh and Elsberry (1993a) found that orographic deflection of a moving TC is more significant with weaker and slower-moving cyclones. A westward-moving cyclone positioned a sufficient distance upstream of a mountain range will decelerate and, subsequently, turn southward when the combined outer cyclone circulation and environmental flow are blocked and deflected by the mountain barrier. As the cyclone further approaches the mountain range, an imbalance in the inner structure of the vortex induces asymmetric flow across the vortex center. This asymmetric flow leads to northward deflection of a cyclone approaching the southern or central parts of the mountain range (e.g., via the ventilation mechanism) and southward deflection of a cyclone approaching the northern part of the mountain. With additional numerical sensitivity experiments, Yeh and Elsberry (1993b) found that more intense and rapidly moving vortices are more likely to cross over a mountain range and follow a continuous track. The studies of Yeh and Elsberry provide further evidence that U, V_{max}, and h can serve as control parameters for determining TC track continuity and deflection.

Using idealized numerical simulations Huang and Lin (1997) and LHHH found that the circulation center of a small typhoon vortex approaching a mountain range tends to be deflected southward, regardless of its strength and translation speed. The southward deflection of the vorticity and low pressure centers can be explained by orographic blocking (LHHH). Similar southward deflection of westward-moving hurricanes impinging upon the Sierra Madre of Mexico has been depicted with shallow-water model experiments (e.g., Zehnder 1993; Zehnder and Reeder 1997). Kuo et al. (2001) also used a shallow-water model to show that, within a quiescent fluid, a vortex becomes trapped near the isolated topography of an island and follows a clockwise, island-circulating path as a result of β effects. However, our rough estimates of the nondimensional parameter R_B, as proposed by Kuo et al. (2001), indicate that topographically induced β effects on impinging cyclones are not significant at the CMR due to the small north–south length scale (L_y) of the mountain range. Hence, the scale of cyclone size (R) and the mountain horizontal scales (L_x, L_y) could also be used in the diagnosis of TC track deflection.

In fact, the problem of tropical cyclones passing over a mountain range is essentially the same for midlatitude cyclones. For example, O'Handley and Bosart (1996) found that 70% of the cyclones approaching the Appalachians from the west or southwest exhibited definite leeside redevelopment in which a distinct and new (secondary) cyclone center appeared at the lee side while the primary cyclone was still evident west of the moun-

tains. Of the redevelopment cases, 79% of secondary cyclones subsequently deepened, with many apparently becoming major cyclones offshore of the Atlantic coast.

In simulating a synoptic-scale vortex advecting toward the Greenland Mountains from the west, Schwierz and Davies (2003) found that the approaching vortex will be redirected poleward around the mountain range. The vortex becomes less (more) discernable at the windward (leeward) side of the mountain range. The subsequent anticyclonic track of the vortex could be a result of influence from an orographically induced anticyclone. Alternatively, the generation of positive vorticity through vorticity stretching within the downsloping sectors of the cyclone circulation may lead to the poleward redirection of the cyclone west of the mountain range and to the formation of a secondary cyclone east of the mountain range and at a latitude south of the primary cyclone (as shown in Fig. 9.9 of Carlson 1998).

Dynamically, the orographic deflection of a moving cyclone results from interaction of topography with the basic flow (Fig. 2a) and the outer cyclone circulation (Fig. 2b). Due to the complicated nonlinear interaction involved, the resulting flow pattern will not be a simple linear superposition of these two flow patterns. For cases of westward-moving tropical cyclones approaching the CMR, the relatively smaller L_y of the CMR of Taiwan may contribute the "cyclonic" deflection of the approaching cyclones, as opposed to "anticyclonic" deflection found with the midlatitude cyclones, independent of influence from the basic flow (e.g., Schwierz and Davies 2003) or outer circulation (Carlson 1998). To thoroughly understand the influence of orography on cyclone track deflection, one needs to understand the significance of the scale of both airflow and mountain range to orographic deflection.

To more accurately predict track continuity and deflection for a TC approaching and traversing a mesoscale mountain, the identification of some major, nondimensional control parameters should prove useful. In this study, we plan to estimate flow and orographic parameters from previous idealized and real-case numerical simulations, as well as observational analyses, to develop control parameters for studying TC track continuity. We then test these prospective control parameters by performing a series of systematic idealized numerical simulations. This paper is organized as follows: Section 2 will feature estimates of flow and orographic parameters from previous studies and propose potential nondimensional control parameters for cyclone track continuity and deflection near the CMR or other topography. In section 3, we will employ a mesoscale model to test prospective control parameters for TC track continuity and deflection associated with the passage of a cyclone over an idealized mesoscale mountain range in the absence of latent heating. Conclusions and a discussion are given in section 4.

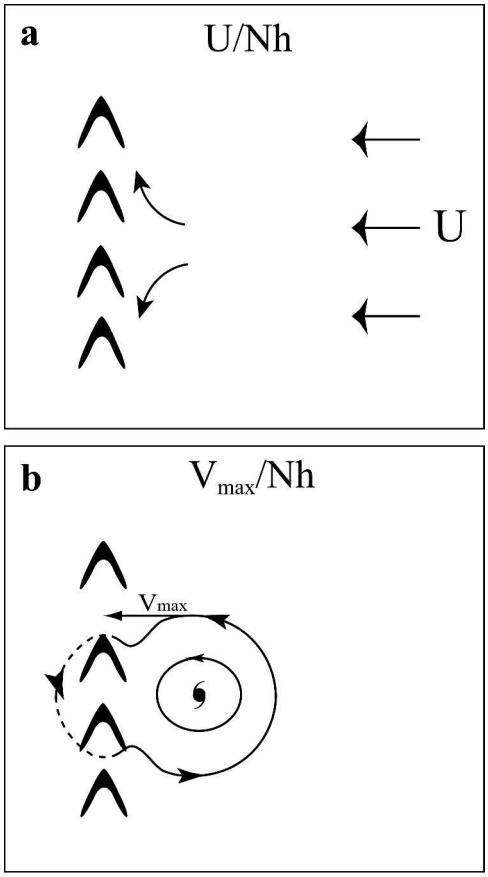

FIG. 2. The effect of orography in deflecting a westward-moving cyclone northward or southward results from the interaction of topography with (a) the basic flow and (b) the outer circulation of the cyclone.

2. Potential control parameters inferred from previous studies

To identify parameters that diagnose the effects of orography to the continuity and deflection of tropical cyclone track over a mesoscale mountain, we estimate flow and orographic parameters from previous studies using idealized and real-case numerical simulations as well as observational analyses. Previous studies selected for this purpose are Wang (1980), Chang (1982), Bender et al. (1987), Yeh and Elsberry (1993a,b), Huang and Lin (1997), LHHH, and Chiao and Lin (2003). The flow and orographic parameters chosen are the basic flow speed (U), the maximum tangential wind speed of the TC (V_{max}), the radius of V_{max} (R), the Brunt–Väisälä frequency (N), the mountain height (h), mountain scales in both the x (L_x) and y (L_y) directions, and the Coriolis parameter (f). The storm depth (D) is not examined here, as a typical tropical cyclone will generally extend through the depth of the troposphere (i.e., 15 to 16 km in altitude). One can safely assume that the depth of any significant TC will be several times greater than a 3-km-high mountain. Thus, we use

V_{max} as a proxy for D. Applying the Buckingham-Π theorem (e.g., Pearson 1983) to the eight dimensional parameters listed above, there exist only six independent nondimensional parameters because there are only the two primary quantities of length and time in the system (see Fig. 2). Based on the schematic representation given in Fig. 2, we may choose the following six nondimensional parameters for possible indicators of track continuity and deflection: V_{max}/Nh, U/Nh, V_{max}/fR, h/L_x, R/L_y, and U/fL_x.

Table 1 summarizes our estimates for control parameters from previous studies. From observational analyses and real-case simulations, U is estimated by averaging the surface to 700-hPa winds. Cyclone track continuity is less sensitive to the magnitudes of R/L_y and U/fL_x. To examine the sensitivity of cyclone track continuity to other parameters, we plot track continuity on parameter spaces, (U/Nh, V_{max}/Nh), (V_{max}/fR, V_{max}/Nh), and (h/L_x, V_{max}/Nh) in Fig. 3, based on previous studies (Table 1). As previously defined, the cyclone track is considered discontinuous (denoted by triangles in Fig. 3) when the upstream cyclone and a lee vortex coexist simultaneously. The track is traced by the maximum vorticity center. Figure 3a indicates that cyclone track continuity is a function of V_{max}/Nh and independent of U/Nh. A transitional boundary between cases of continuity and discontinuity can be discerned at $V_{max}/Nh = 1.5$. One could argue that a different boundary exists such that V_{max}/Nh increases with increasing values of U/Nh and with cases 8 and 13 being opposite to cases 10 and 14. However, the range of U/Nh calculated from previous studies may be too narrow to justify this boundary placement. This relationship will be further examined in a broader parameter space with idealized simulations. The same transitional boundary of $V_{max}/Nh = 1.5$ can also be discerned from Figs. 3b and 3c, particularly if case 13 is discounted. Thus, we hypothesize that cyclone track continuity is mainly controlled by V_{max}/Nh, and is less sensitive to the other parameters, such as U/Nh, V_{max}/fR, h/L_x, R/L_y, and U/fL_x.

The nondimensional control parameter V_{max}/Nh may be regarded as a vortex Froude number for the outer circulation of a cyclone, analogous to the basic-flow Froude number (U/Nh). The nondimensional control parameter V_{max}/fR, may be regarded as a measure of the Lagrangian Rossby number for the cyclone circulation or the nondimensional vorticity of the cyclone, while another control parameter, h/L_x, measures the steepness of the mountain barrier. The nondimensional control parameters R/L_y is the ratio of the cyclone scale to the scale of the mountain range in a direction normal to cyclone motion, and U/fL_x is the Rossby number associated with the basic flow.

As a TC vortex encounters a north–south oriented mountain range (such as the CMR) from the east, the northern half of the vortex circulation impinges upon the mountain range perpendicularly, as depicted in the sketch of Fig. 2b. The vortex Froude number V_{max}/Nh,

TABLE 1. Parameters estimated from previous studies of tropical cyclones traversing the CMR of Taiwan. 1) CL: Chiao and Lin (2003); 2) HL5: Huang and Lin (1997) ($V_{max} = 20$ m s^{-1}); 3) HL10: Same as 2) but with $U = 10$ m s^{-1}; 4) Lin: Lin et al. (1999); 5) Ch3: Chang (1982) with $V_{max} = 16$ m s^{-1}; 6) WG2: Wang (1980) with $V_{max} = 36.8$ m s^{-1}; 7) W1S: YE's case W1S; 8) W1Ss: Same as 7) but with $U = 2.5$ m s^{-1}; 9) CN15: Simulated case in Lin et al. (2002); 10) HL40: Same as 2) but with $V_{max} = 40$ m s^{-1}; 11) WG1: Same as 6) with $V_{max} = 52.4$ m s^{-1}; 12) B5: Bender et al. (1987) with $U = 5$ m s^{-1}; 13) B10: Same as 12) but with $U = 10$ m s^{-1}; 14) Ch2: Same as 5) but with $V_{max} = 30$ m s^{-1}; 15) IIS: YE's case; 16) Bilis: Observed case in Lin et al. (2002). Here C and D denote continuous and discontinuous tracks, respectively.

Case		U (m s^{-1})	V_{max} (m s^{-1})	N (0.01 s^{-1})	h (km)	R (km)	L_x (km)	L_y (km)	f (10^{-5} s^{-1})	Deflection	C/D	V_{max}/Nh	U/Nh	V_{max}/Rf	h/L_x	R/L_y	U/fL_x
1	CL	5	15.6	.98	3.0	110	75	180	5.8	~0	D	0.52	0.160	2.46	0.040	0.61	1.15
2	HL5	5	20.0	1.025	2.5	120	100	150	5.0	S	D	0.78	0.195	3.33	0.025	0.80	1.00
3	HL10	10	20.0	1.025	2.5	120	100	150	5.0	S	D	0.78	0.390	3.33	0.025	0.80	2.00
4	Lin	10	20.0	1	2.5	180	80	240	5.8	S	D	0.80	0.400	1.92	0.031	0.75	2.16
5	Ch3	5	16.0	0.72	2.0	210	120	240	5.0	N	D	1.11	0.347	1.52	0.017	0.88	0.83
6	WG2	5	36.8	0.98	3.0						D	1.23					
7	W1S	5	19.0	0.51	2.5	135	160	205	5.8	N	D	1.49	0.390	2.43	0.016	0.66	0.54
8	W1Ss	2.5	19.0	0.51	2.5	135	160	205	5.8	N	D	1.49	0.195	2.43	0.016	0.66	0.27
9	CN15	6	35.0	0.78	3.0	200	75	180	5.8	N	D	1.50	0.256	3.02	0.040	1.11	1.37
10	HL40	5	40.0	1.025	2.5	120	100	150	5.0	S	C	1.56	0.195	6.67	0.025	0.80	1.00
11	WG1	5	52.4	0.98	3.0						C	1.75					
12	B5	5	50.0	0.86	3.0	200	80	190	5.8	N+	C	1.94	0.194	4.31	0.038	1.05	1.08
13	B10	10	50.0	0.86	3.0	200	80	190	5.8	~0	D	1.94	0.388	4.31	0.038	1.05	2.16
14	Ch2	5	30.0	0.72	2.0	210	120	240	5.0	N	C	2.08	0.347	2.86	0.017	0.88	0.83
15	IIS	5	33.0	0.51	2.5	135	160	205	5.8	N-	C	2.59	0.390	4.22	0.016	0.66	0.54
16	Bilis	5	72.0	0.89	3.0	200	75	180	5.8	N	C	2.70	0.187	6.21	0.040	1.11	1.15

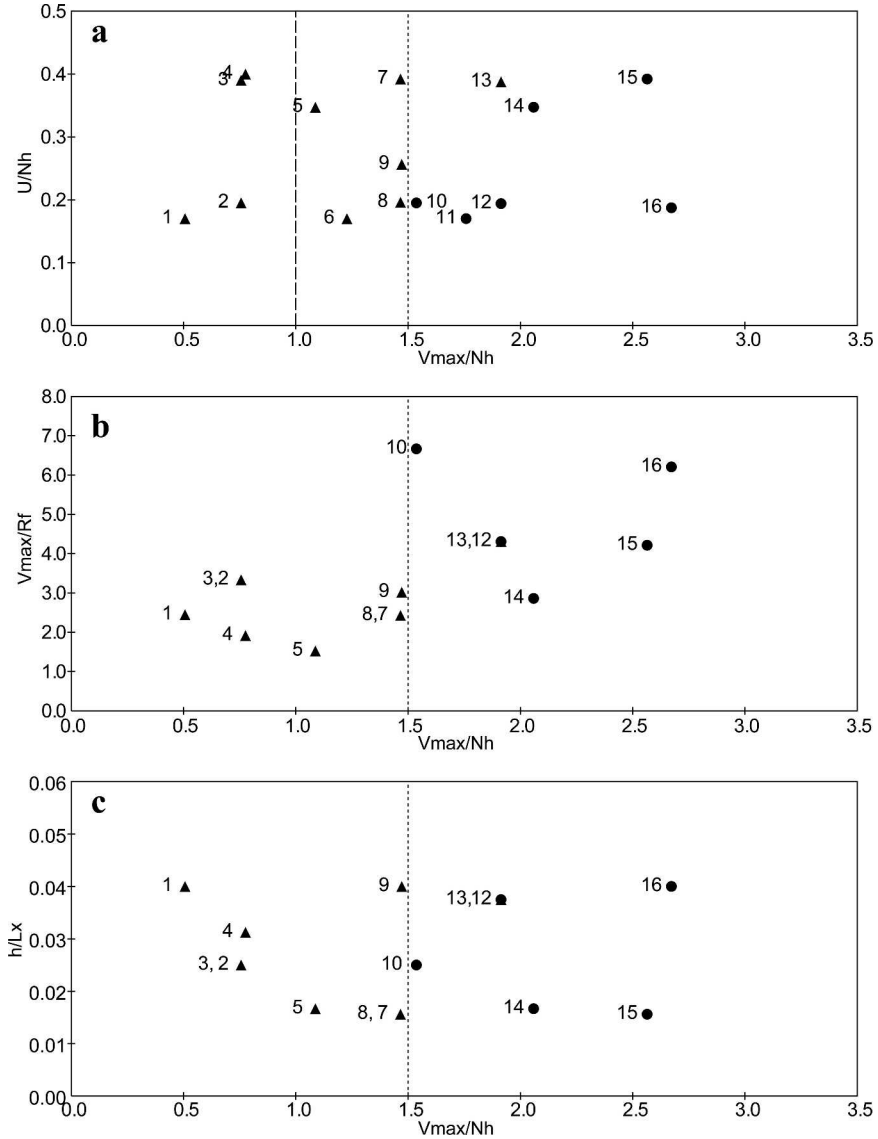

FIG. 3. Continuous (filled circles) and discontinuous (triangles) cyclone tracks in the parameter spaces of (a) (U/Nh, V_{max}/Nh), (b) (V_{max}/fR, V_{max}/Nh), and (c) (h/L_x, V_{max}/Nh), based on previous studies of tropical cyclones over CMR or its idealized topography. The track is continuous (discontinuous) for cases to the right (left) of the dotted lines (V_{max}/Nh = 1.5). Cyclone tracks indicated to the right (left) of the dashed line at V_{max}/Nh = 1.0 in (a) were deflected northward (southward). Case numbers are denoted near the symbols and the associated parameters are listed in Table 1.

therefore, can be used as a localized measure of orographic blockage of cyclone air passage over a mountain barrier. When V_{max}/Nh is small, orographic blocking of cyclone air parcels is stronger, and the air parcels will be forced around the mountain barrier. A TC vortex would be blocked at the mountain range, and the subsequent track of the TC vortex would be discontinuous. Conversely, when V_{max}/Nh is large, orographic blocking is weak and the TC vortex track tends to be more continuous. These phenomena are analogous to the flow-around and flow-over regimes, respectively, for three-dimensional dry flow over an isolated mountain (e.g., Smolarkiewicz and Rotunno 1989; Smith and Gronas 1993).

Table 1 indicates that the northward or southward track deflection with a westward-moving TC is related only to V_{max}/Nh, if case 10 is discounted. When V_{max}/Nh is greater (less) than unity, a TC tends to be deflected northward (southward). This hypothesis is consistent with LHHH and with Huang and Lin (1997). Aside from the influence of the cyclone circulation in cyclone deflection, several idealized numerical simula-

tions (e.g., Chang 1982; Bender et al. 1987; Yeh and Elsberry 1993a, b) have indicated that the TC track is strongly influenced by the steering (basic) flow, which may be represented by the basic-flow Froude number (U/Nh). However, the dependence of TC track deflection on U/Nh has not been clearly distinguished in the parameter analysis of previous studies (Table 1), and will be examined in the next section.

3. Verification of potential control parameters for track continuity and deflection

a. The model and experiment design

In this study, we employ a mesoscale numerical model (NCSU-GFDM; LHHH) to determine the dominant control parameters for the continuity of a cyclone track over an idealized, mesoscale mountain range. The major characteristics of the model are summarized as follows:

- The time-dependent, hydrostatic governing equations are solved on an Arakawa-C staggered grid.
- The third-order Adams–Bashforth scheme is used for time marching.
- The horizontal (vertical) advection terms are approximated using quadratic conservative fourth- (second-) order-centered finite difference.
- A terrain-following ($\sigma - z$) vertical coordinate is adopted, where σ is defined as $\sigma = z_T(z - h)/(z_T - h)$. Here z_T and h are the heights of the computational domain and terrain elevation, respectively.
- A free-slip lower-boundary condition is used.
- A radiation upper-boundary condition is used.
- The horizontal domain average is subtracted from perturbation pressure fields in every grid point at every time step.
- A five-point numerical smoother for diffusion is applied.
- Latent heating is excluded in all simulations.

Details of the numerical formulation of the model can be found in LHHH and Han (1998).

For most cases presented here, a uniform, stably stratified basic flow is introduced instantaneously at nondimensional time $Ut/a = 0$. The Brunt–Väisälä frequency is set as $N = 0.01\ \mathrm{s}^{-1}$ for all experiments performed in this study. An f-plane approximation has also been made, where the Coriolis parameter f_o is taken to be $5.8 \times 10^{-5}\ \mathrm{s}^{-1}$. The flow is inviscid throughout the entire model domain. The vertical grid interval is 500 m, while the horizontal grid interval is $\Delta x = \Delta y = 30$ km. The numbers of grid points in the x, y, and z directions are $151 \times 121 \times 31$ for a domain size of 4500 km 3600 km $\times$ 15 km. The idealized, bell-shaped topography is prescribed as

$$h(x, y) = \frac{h}{[(x/a)^2 + (y/b)^2 + 1]^{3/2}}, \qquad (1)$$

where h is the mountain height and a and b are the mountain half-widths in the x and y directions, respectively. For most cases, we have used $a = 40$ km and $b = 120$ km, which are comparable to those of CMR. Note that we use $2a$ and $2b$ to roughly represent L_x and L_y, respectively.

An idealized cyclone is initialized with a prescribed tangential velocity following LHHH and Chang (1982),

$$v_\theta = v_{\max}\left(\frac{r}{r_{\max}}\right)\exp\left\{\frac{1}{2}\left[1 - \left(\frac{r}{r_{\max}}\right)^2\right]\right\}, \qquad (2)$$

where $v_{\max}$ is the maximum tangential velocity at a radius of $r_{\max}$ from the cyclone center. The details of the model initialization procedure can be found in LHHH. The horizontal structures of the surface perturbation pressure, surface vertical vorticity, and vector wind fields at $Ut/a = 0$ roughly correspond to the fields shown by LHHH Fig. 7, $Ut/a = 10$, while the perturbation pressure and θ fields over a cross section of $y/a = 0$ are identical to Figs. 9a and 9b, respectively inLHHH. As latent heating effects were not used in this study, simulated cyclone vortices were prescribed with relatively large radii of maximum wind (R), in order to ensure barotropic stability with the simulated vortex. The vortex is initially located at $x/a = -12.5$ for all cases except for the quiescent fluid case in which the vortex is first located at $x/a = -5$.

b. Verification of some potential control parameters for track continuity and deflection

Based on the previous studies analyzed in the last section, six potential control parameters, ($V_{\max}/Nh$, U/Nh, $V_{\max}/fR$, h/L_x, R/L_y, and U/fL_x) are tested through a series of idealized numerical experiments. The flow and orographic parameters used for these experiments are listed in Table 2. Cyclone tracks are discontinuous for all A and B cases, which have $U/fL_x = 0.539$ to 3.233; cyclone tracks are continuous for all D and E cases, and have $U/fL_x = 0.539$ to 2.155. Thus, the track continuity is not sensitive to the basic-flow Rossby number, U/fL_x.

The dependencies of track continuity on U/Nh, $V_{\max}/fR$, h/L_x, R/L_y versus $V_{\max}/Nh$ are plotted in Fig. 4. Cyclone track continuity is less sensitive to U/Nh, $V_{\max}/fR$, h/L_x, and R/L_y, and is dominated by $V_{\max}/Nh$. A critical zone for cyclone track continuity may be drawn at $V_{\max}/Nh = 1.2$ to 1.6. With $V_{\max}/Nh < 1.2$, a cyclone track will tend to be discontinuous; with $V_{\max}/Nh > 1.6$, a cyclone track will tend to be continuous. Although a critical zone of $V_{\max}/Nh$ is used rather than a critical boundary of $V_{\max}/Nh = 1.5$ (as shown in Fig. 3) to depict the transition of continuous and discontinuous cyclone tracks, the results of the model simulations largely agree with those of the previous studies. Thus, we found that continuity of a cyclone track over a mesoscale mountain range is mainly controlled by $V_{\max}/Nh$ for the current setting of basic flow, orographic and vortex. Dynamically, this indicates that, when orographic blocking of the impinging cyclone is strong

TABLE 2. Parameters used for testing cyclone track continuity and deflection in idealized simulations. Constant values of $N = 0.01$ s^{-1}, $L_x = 80$ km, and $f = 5.8 \times 10^{-5} s^{-1}$ are used for all cases: C and D denote continuous and discontinuous tracks, respectively.

Case	V_{max}	h (km)	R (km)	U	L_x (km)	L_y (km)	V_{max}/Nh	U/Nh	V_{max}/fR	h/L_x	R/L_y	U/fL_x	C/D
A2	20	4.00	180	10.0	80	240	0.50	0.25	1.92	0.050	0.750	2.155	D
A4	20	4.00	180	5.0	80	240	0.50	0.13	1.92	0.050	0.750	1.078	D
A8	20	4.00	180	2.5	80	240	0.50	0.06	1.92	0.050	0.750	0.539	D
B1	20	2.50	180	15.0	80	240	0.80	0.60	1.92	0.031	0.750	3.233	D
B2	20	2.50	180	10.0	80	240	0.80	0.40	1.92	0.031	0.750	2.155	D
B4	20	2.50	180	5.0	80	240	0.80	0.20	1.92	0.031	0.750	1.078	D
B8	20	2.50	180	2.5	80	240	0.80	0.10	1.92	0.031	0.750	0.539	D
C2	20	1.60	180	10.0	80	240	1.25	0.63	1.92	0.020	0.750	2.155	D
C4	20	1.60	180	5.0	80	240	1.25	0.31	1.92	0.020	0.750	1.078	C
C8	20	1.60	180	2.5	80	240	1.25	0.16	1.92	0.020	0.750	0.539	C
C10	20	1.60	180	2.0	80	240	1.25	0.13	1.92	0.020	0.750	0.431	D
D2	20	1.00	180	10.0	80	240	2.00	1.00	1.92	0.013	0.750	2.155	C
D4	20	1.00	180	5.0	80	240	2.00	0.50	1.92	0.013	0.750	1.078	C
D8	20	1.00	180	2.5	80	240	2.00	0.25	1.92	0.013	0.750	0.539	C
D10	20	1.00	180	2.0	80	240	2.00	0.20	1.92	0.013	0.750	0.431	C
E2	20	1.25	180	10.0	80	240	1.60	0.80	1.92	0.016	0.750	2.155	C
E4	20	1.25	180	5.0	80	240	1.60	0.40	1.92	0.016	0.750	1.078	C
E8	20	1.25	180	2.5	80	240	1.60	0.20	1.92	0.016	0.750	0.539	C
E10	20	1.25	180	2.0	80	240	1.60	0.16	1.92	0.016	0.750	0.431	C
F1	20	2.50	180	10.0	80	240	0.80	0.40	1.92	0.031	0.750	2.155	D
F2	30	3.75	180	5.0	80	240	0.80	0.13	2.87	0.047	0.750	1.078	D
F3	30	3.75	120	2.0	80	240	0.80	0.05	4.31	0.047	0.500	0.431	D
F4	20	1.00	180	10.0	80	240	2.00	1.00	1.92	0.013	0.750	2.155	C
F5	30	1.50	180	5.0	80	240	2.00	0.33	2.87	0.019	0.750	1.078	C
F6	30	1.50	120	2.0	80	240	2.00	0.13	4.31	0.019	0.500	0.431	C
F7	20	0.80	180	10.0	80	240	2.50	1.25	1.92	0.010	0.750	2.155	C
F8	30	1.00	180	5.0	80	240	3.00	0.50	2.87	0.013	0.750	1.078	C
F9	30	1.00	120	2.0	80	240	3.00	0.20	4.31	0.013	0.500	0.431	C
F10	20	2.00	250	10.0	80	240	1.00	0.50	1.38	0.025	1.042	2.155	D
F11	20	1.00	250	5.0	80	240	2.00	0.50	1.38	0.013	1.042	1.078	C
F12	20	0.80	250	2.0	80	240	2.50	0.25	1.38	0.010	1.042	0.539	C
G1	30	3.75	90	5.0	80	240	0.80	0.13	5.75	0.047	0.375	1.078	D
G2	30	3.75	90	5.0	80	480	0.80	0.13	5.75	0.047	0.188	1.078	D
G3	30	1.5	90	5.0	80	240	2.00	0.33	5.75	0.019	0.375	1.078	C
G4	20	1.25	90	10.0	80	360	1.60	0.80	3.83	0.016	0.250	2.155	D
H1	30	3.75	180	5.0	80	240	0.80	0.13	2.87	0.047	0.750	1.078	D
H2	30	3.75	180	5.0	80	240	0.80	0.13	2.87	0.047	0.750	1.078	D
Q	20	2.50	180	0.0	80	240	0.80	0.00	1.92	0.031	0.750	0.000	D

(weak), the cyclone track tends to be discontinuous (continuous).

Given smaller values of V_{max}/Nh and U/Nh, deflection of the cyclone track will be greater near a mesoscale mountain range (Table 2; Fig. 5). Dynamically, this implies that the greater the orographic blocking, the greater the deflection of the moving cyclone near a mesoscale mountain range. For the parameter spaces used in Fig. 4 and Table 2, nearly all incoming vortices are deflected to the north upstream of the mountain range, except when a cyclone is very close to the mountain range. As will be discussed later, the relatively large radii of the vortices simulated in our experiments do affect the results of these idealized experiments. Simulated vortices with a smaller, more realistic radius will tend to be deflected southward, consistent with experiments by Huang and Lin (1997) and by LHHH. For cases with smaller values of U/Nh and V_{max}/Nh, such as case F2, more low-level air parcels of the cyclone are blocked by the mountain range and are forced to go around the northern slope of the idealized mountain range, and the cyclone is deflected farther to the north as it draws nearer to the mountain range (Fig. 6a). Concurrently, a secondary vortex is produced on the lee side of the mountain range. Both the parent and lee vortices are associated with strong vorticity maxima upstream and downstream of the mountain range, respectively (Figs. 7b and 7c). For cases with larger values of U/Nh and V_{max}/Nh, such as case F11 (Fig. 6c), more low-level air parcels of the parent cyclone pass over the mountain range directly, so the cyclone is not deflected to the north to the extent that the cyclone is in case F2. Note that the circulation center of case F11 is deflected southward, while the vorticity center is being deflected

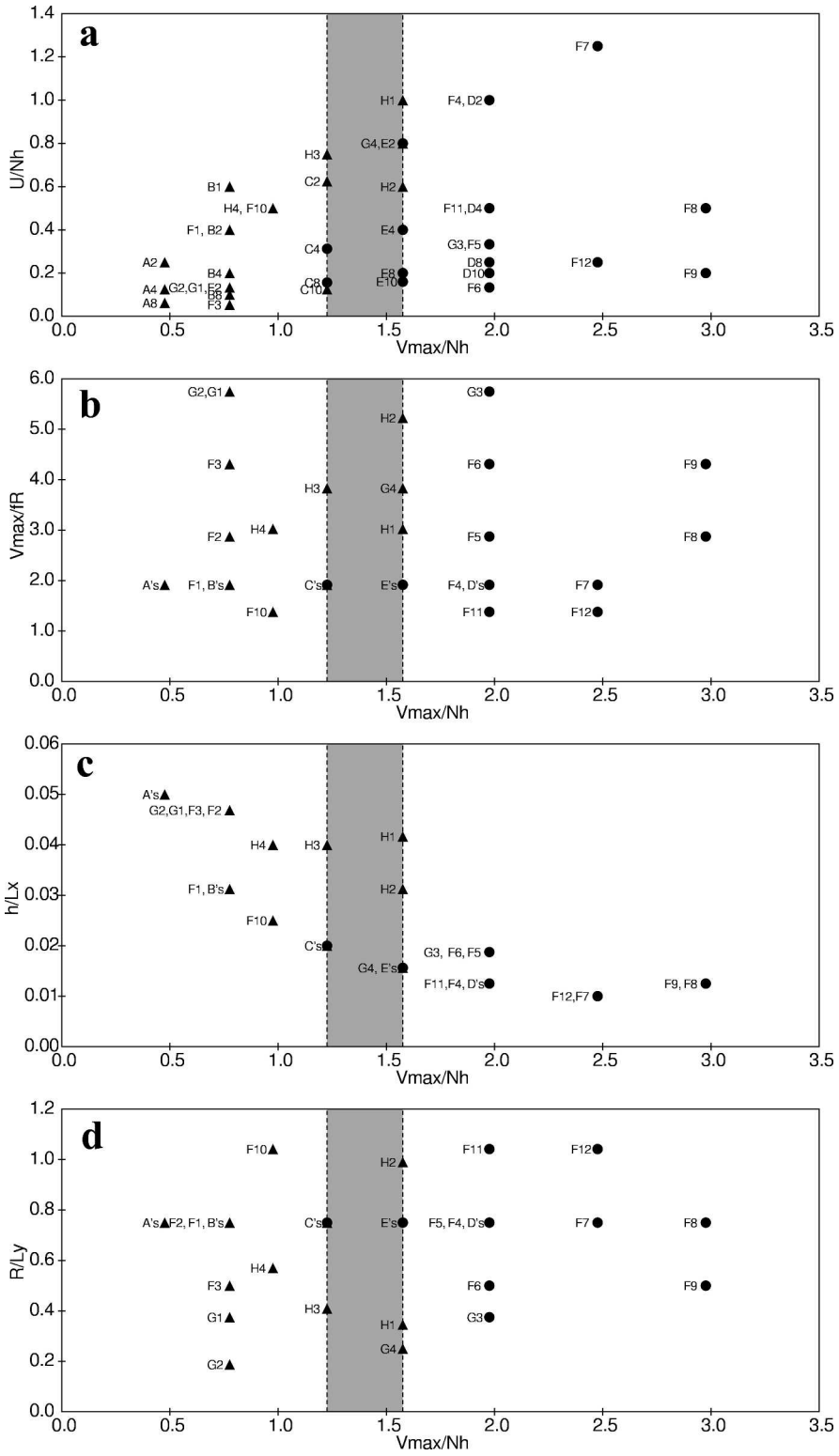

FIG. 4. (a)–(c) As in Fig. 3 except for idealized simulations; (d) track continuity regime in the parameter space of (R/L_y, V_{max}/Nh). The proposed critical zone for cyclone track continuity is denoted by the gray-shaded block. This figure indicates that a cyclone track becomes discontinuous (continuous) when V_{max}/Nh is small (large).

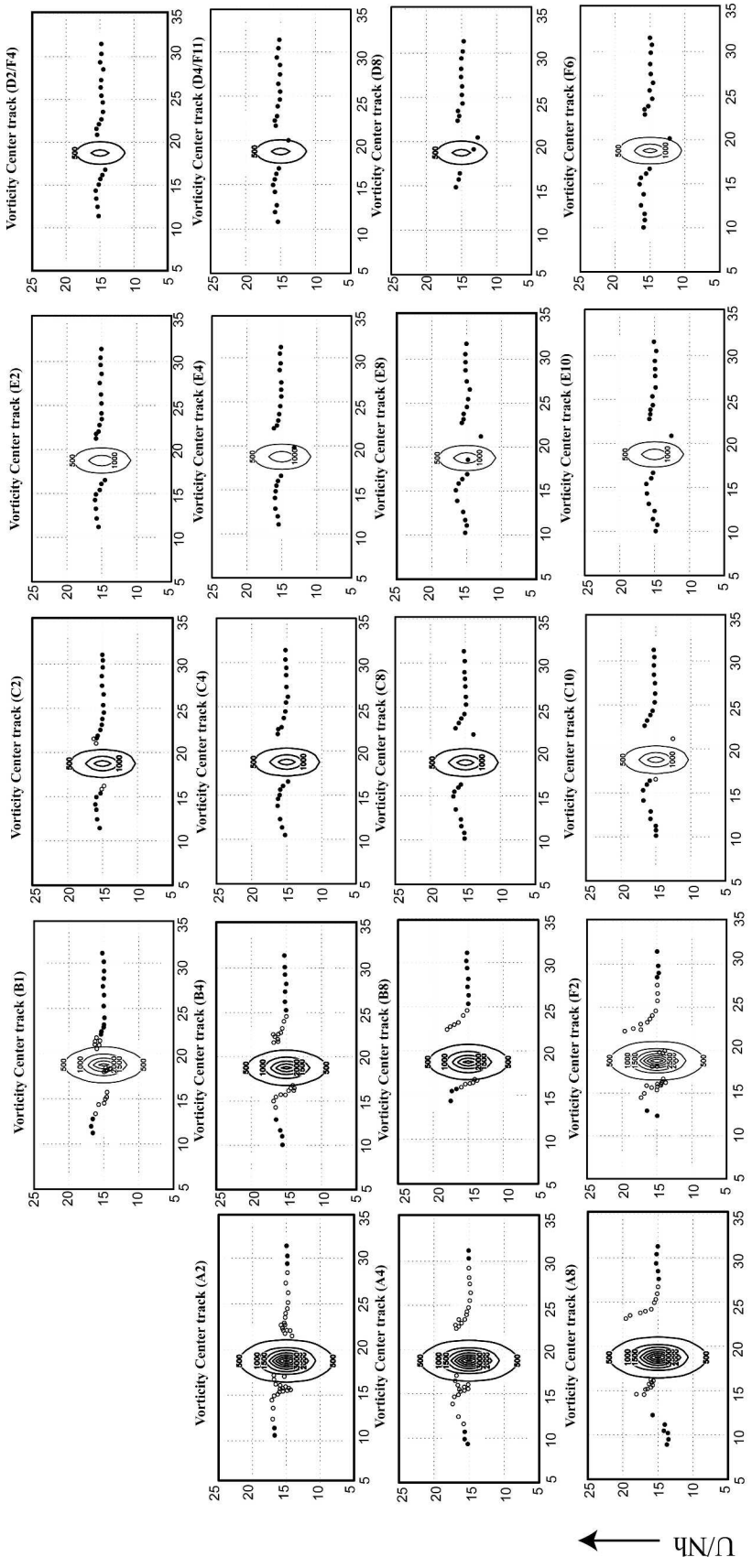

FIG. 5. Selected vorticity center tracks from idealized simulations. Figure panels are arranged so that U/Nh and V_{max}/Nh increase upward and rightward, respectively. Both dimensional and nondimensional parameters can be found in Table 2. Outlined circles represent coexisting vorticity centers on both the upstream and downstream side of the mountain. The axes in the x and y direction are nondimensionalized by a, the half-width of the mountain in x direction. Nondimensional axes are used in all figures depicting a horizontal plane hereafter.

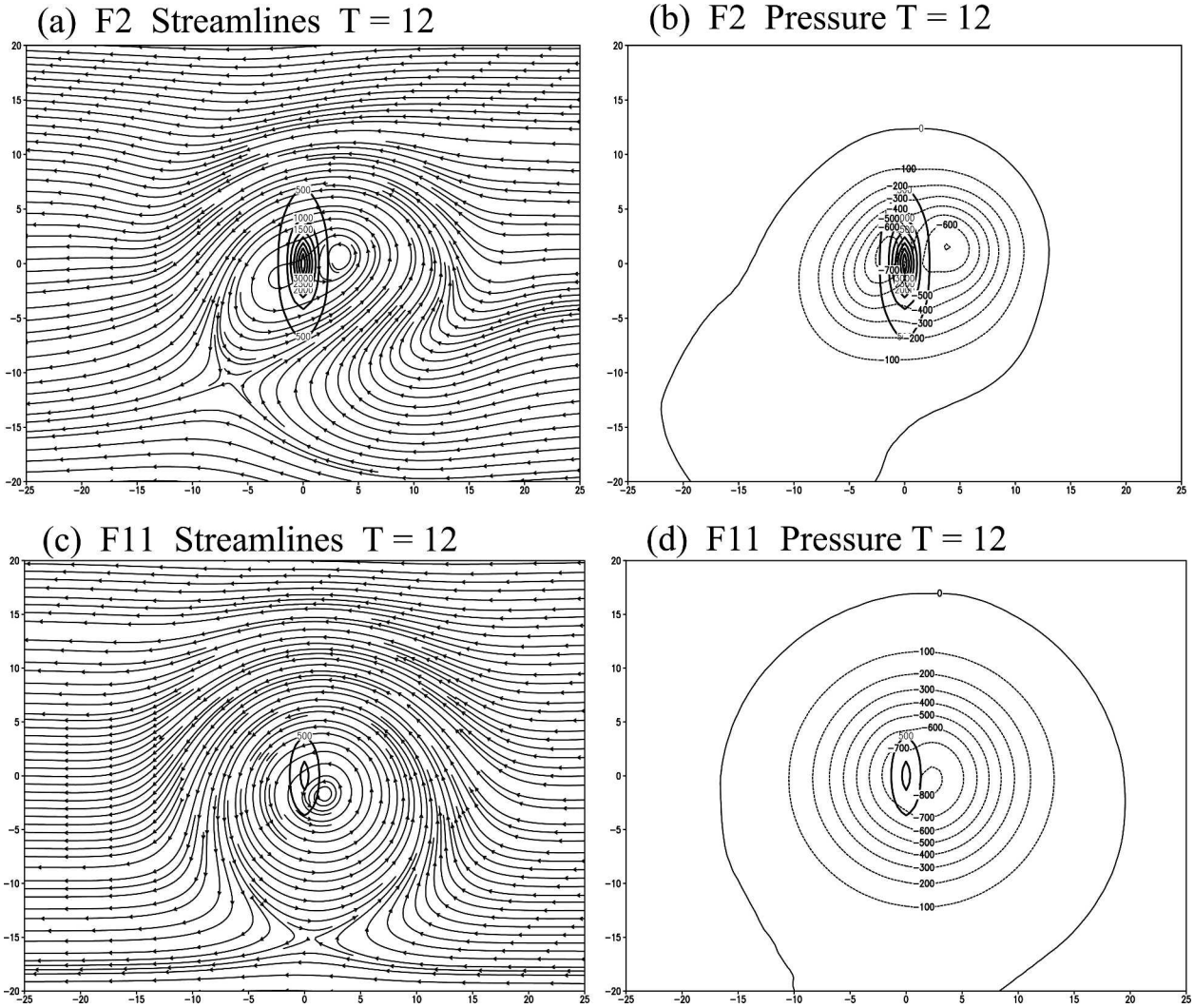

FIG. 6. NCSU GFD Model simulated (a) streamline and (b) perturbation pressure (in Pa) fields for case F2 at σ = 250 m for an idealized cyclone embedded within easterly flow at the nondimensional time Ut/a = 12. (c), (d) Similar to (a), (b), respectively, except for case F11. Terrain contour interval is 500 m. Nondimensional control parameters (V_{max}/Nh, U/Nh, R/L_y) are (0.8, 0.13, 0.75) for F2 and (2.0, 0.5, 1.042) for F11. Cases F2 and F11 represent moderate and weak blocking cases, respectively.

northward (Fig. 8a). The perturbation pressure fields for cases F2 and F11 are shown in Figs. 6b and 6d, respectively. Roughly speaking, maximum vorticity regions are associated with low pressure. However, the lee vortex in case F2 is not collocated with the low pressure center, as the secondary, leeside low pressure center initially forms through adiabatic heating associated with downslope wind, as is described by Lin (1993), LHHH, and Wu and Kuo (1999). The lee vortex and the secondary low eventually merge and develop into a cyclone, replacing the original cyclone.

Figure 7 shows the relative vertical vorticity fields of Case F2 for Ut/a = 6, 9, 12, and 15. For Ut/a = 6, the vortex center is located at y = 0 km and is not yet significantly influenced by the mountain range. However, air parcels contained in the outer circulation of the cyclone are blocked by the mountain range, and the vorticity field is skewed northward by vorticity advection (LHHH). For Ut/a = 9, when the vortex is nearer to the mountain range, much of the associated low-level flow is forced around the northern end of the mountain range. The cyclone scale (R = 180 km) is comparable to the mountain scale normal to the basic flow (L_y = 240 km), and the continued redirection of the outer circulatory flow of the cyclone around the northern end of the mountain range will result in enhanced northward vorticity advection and consequent northward cyclone deflection of the cyclone in this case of moderate orographic blocking. Midlevel circulatory flow passes over the mountain range directly and slopes down the lee side, where vorticity stretching is induced (LHHH). For Ut/a = 12, vorticity of the lee vortex increases to a

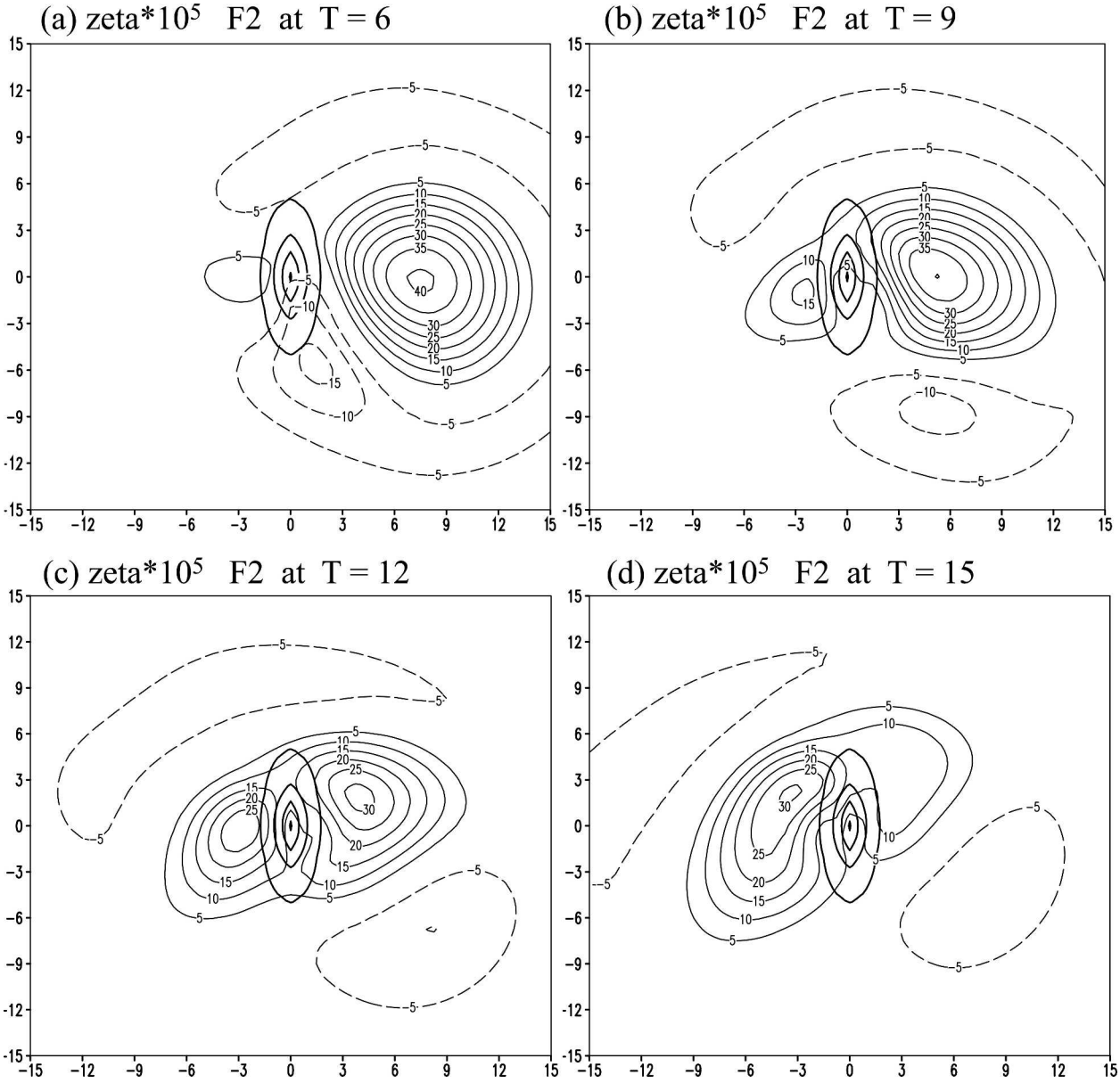

FIG. 7. Relative vertical vorticity field for case F2 at Ut/a = (a) 6, (b) 9, (c) 12, and (d) 15. Vorticity is contoured every 5×10^{-5} s^{-1}, with dashed contours representing negative values. Oval contours centered around $x = 0$ and $y = 0$ are terrain every 1000 m. Only a subset of the actual computational domain is plotted.

value of 2.5×10^{-5} s^{-1}, comparable to that of the parent vortex (3.0×10^{-5} s^{-1}). For $Ut/a = 15$, vorticity of the lee vortex further increases to 3.0×10^{-5} s^{-1}, and the lee vortex then replaces the parent cyclone. This process occurs over a relatively short span of time; therefore, discontinuity is introduced to the cyclone track. Note that the southern portion of the outer circulation associated with the secondary lee vortex may contribute to the generation of an additional, secondary, vortex to the southeast (upstream) of the mountain range. This development of vorticity to the southeast may account for an abrupt southward displacement of a cyclone approaching the mountain range, as seen with cases A2, C8, C10, E8, E10, D4/F11, D8, and F6 (Fig. 5). Apparently, orographic blocking is a strong determining factor of whether a cyclone track is to be continuous or discontinuous. The relatively strong blocking of case F2 is measured by $V_{\max}/Nh = 0.8$, $U/Nh = 0.13$, and $R/L_y = 0.75$. Whether orographic blocking is a product of the interaction of topography with the basic flow or with the outer cyclone circulation is a topic to be addressed in section 3c.

The behavior of the cyclone in case F11 is very different from that of the cyclone in case F2 (Fig. 7). Fig-

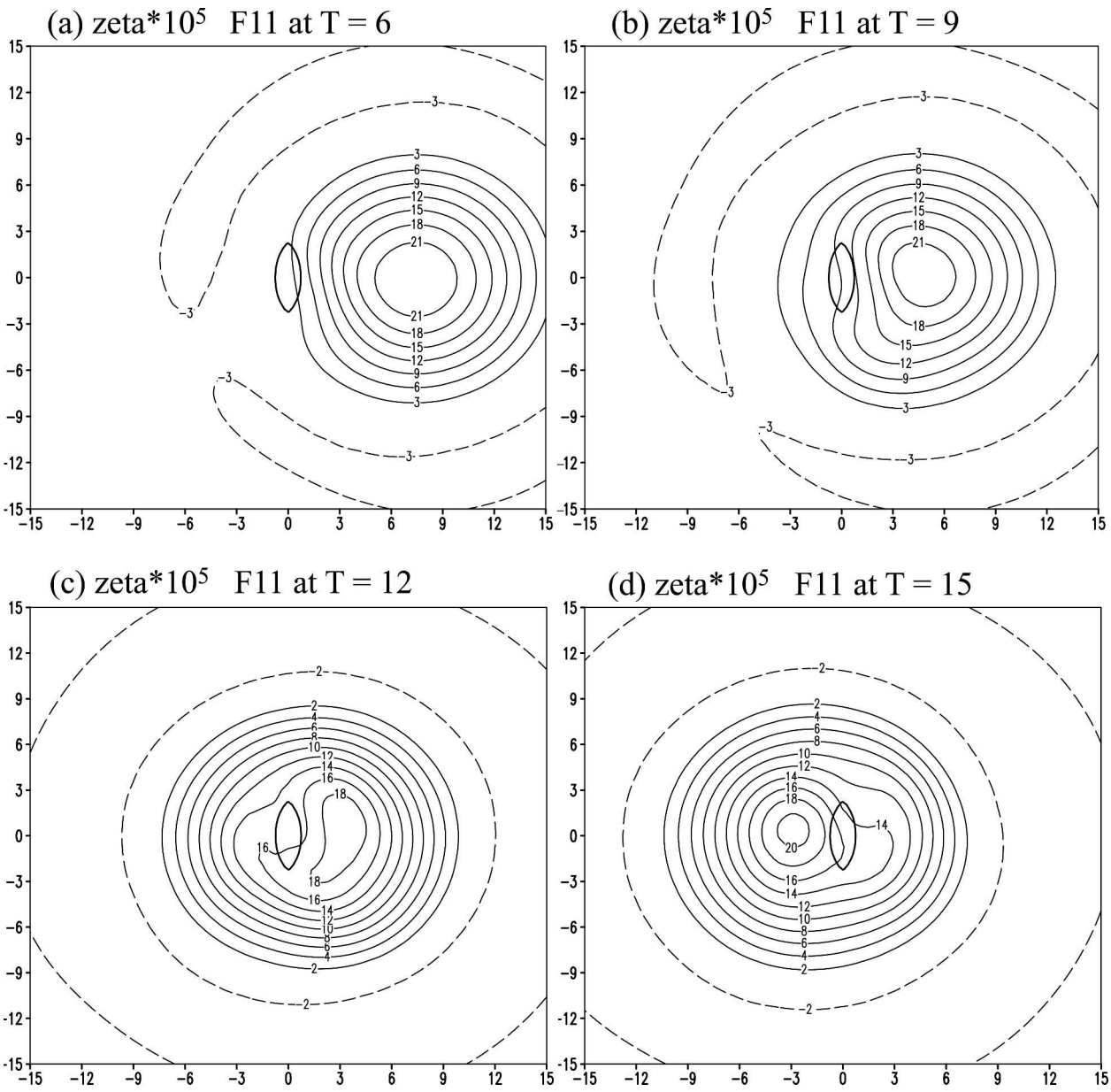

FIG. 8. As in Fig. 7 except for case F11 and with vorticity contoured every 2×10^{-5} s^{-1}.

ure 8 shows the relative vertical vorticity fields for case F11 at Ut/a = 6, 9, 12, and 15. Three major differences are that a) the cyclone track is continuous; b) there is no lee vortex coexisting with the parent cyclone; and c) although the cyclone is still being deflected to the north, the deflection is much smaller. The differences are due to the weaker blocking exerted by the mountain range on the drifting cyclone for case F11, allowing more airflow over the mountain range. The weaker blocking for case F11 is measured by (V_{max}/Nh, U/Nh, R/L_y) = (2.0, 0.5, 1.042), compared to (V_{max}/Nh, U/Nh, R/L_y) = (0.80, 0.13, 0.750).

As discussed in the introduction, Huang and Lin (1997) and LHHH found that a simulated small ($R \ll L_y$), westward-moving cyclone tends to be deflected southward when approaching idealized CMR from upstream, regardless of the intensity and translation speed of the cyclone. The dynamical problem for a small cyclone traversing the idealized CMR is analogous to a hurricane passing over a much larger mountain range, such as the Sierra Madre of Mexico (Zehnder 1993; Zehnder and Reeder 1997). This may be attributed to the inherently strong blocking effects of a larger and longer mountain range. With the scale of the cyclone measured by R and the scale of the mountain perpendicular to direction of cyclone movement mea-

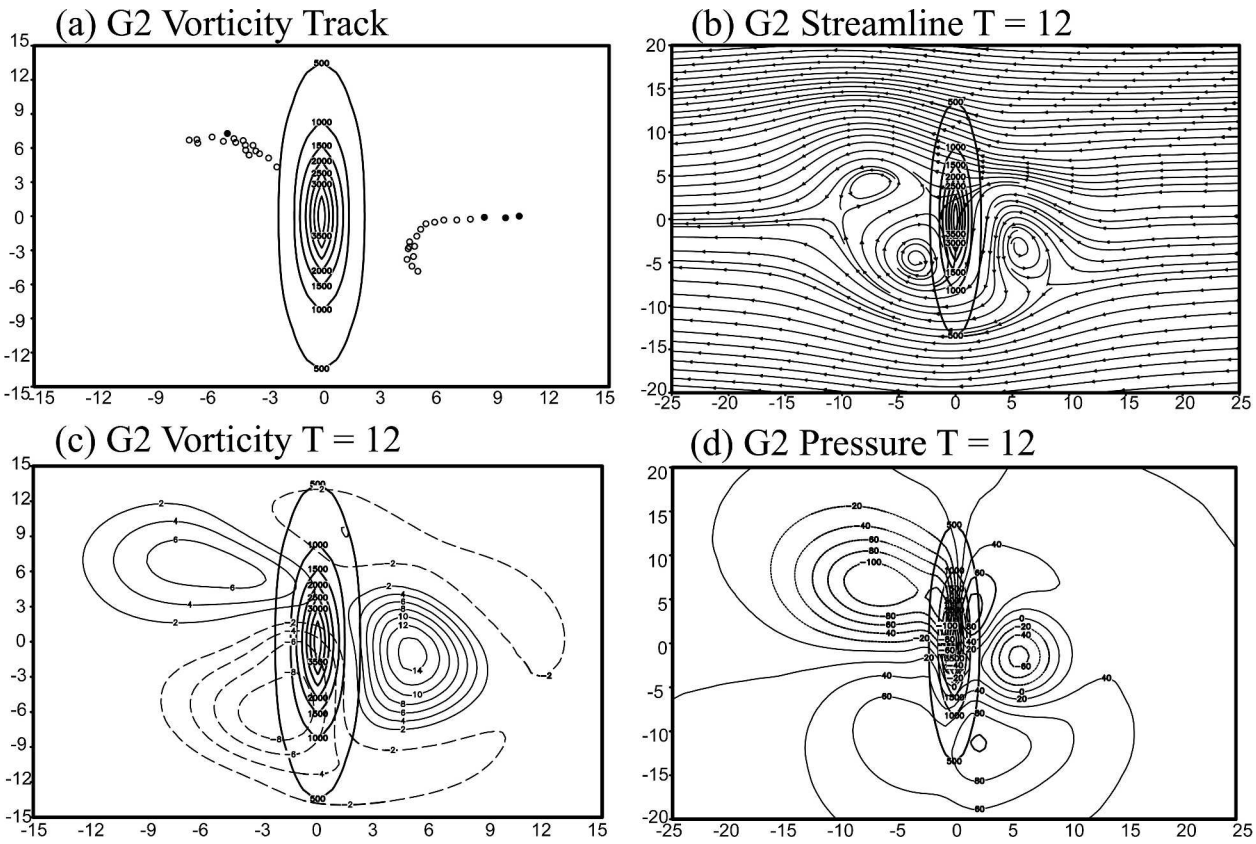

FIG. 9. (a) Track, (b) streamlines, (c) vorticity, and (d) perturbation pressure fields at $Ut/a = 12$ for case G2. The flow and orographic parameters of case G2 is identical to case F2 except R/L_y is significantly reduced, i.e., $(V_{max}/Nh, U/Nh, R/L_y) = (0.8, 0.13, 0.188)$.

sured by L_y, the parameter R/L_y could also be used to diagnose the degree of TC track deflection northward or southward as well as the track continuity. We test the idea that the effects of orographic blocking may also be controlled by other nondimensional parameters, such as R/L_y and U/Nh, along with V_{max}/Nh. To investigate the sensitivity of this parameter, we perform four additional experiments with $(V_{max}/Nh, U/Nh, R/L_y) =$: (i) 0.8, 0.13, 0.375; case G1; (ii) 0.8, 0.13, 0.188; case G2; (iii) 2.0, 0.33, 0.375; case G3; and (iv) 1.6, 0.8, 0.25; case G4.

Figure 9 shows the vorticity center track along with the streamline, vorticity, and perturbation pressure fields at $Ut/a = 12$ for case G2. Note that G2 represents a strong blocking case, compared to the moderate blocking case of F2 and the weak blocking case of F11. Similar to F2, a secondary cyclonic vortex forms on the lee side of the mountain range while the parent cyclone is located far upstream (Fig. 9a). However, one significant difference from case F2 is that the upstream vorticity center is deflected southward. Since both vorticity centers exist simultaneously (Fig. 9b), the track of this simulated cyclone is categorized as discontinuous. An anticyclonic vortex forms on the southwest slope of the mountain range. The blocking of the basic flow and the circulation of the parent cyclone at the mountain range appears to result in vortex shedding on the lee side, similarly found with vertically uniform flow over a mesoscale mountain (e.g., Sun et al. 1991; Lin et al. 1992). These shed vortices are depicted as the vorticity maxima and minima in Fig. 9c. The secondary cyclonic vortex at this time is collocated with a low-pressure center (Fig. 9d), so the main cyclone position is relocated with the secondary vortex. Between the original parent cyclone and the mountain range, strong blocking has contributed to the development of a strong northerly jet (Fig. 9b). As was pointed out by LHHH, the presence of this jet is crucial for the vorticity advection to the east of the mountain range and south of the centerline of $y/a = 0$; the parent cyclone is, therefore, redirected southward (Fig. 9a).

Figure 10 shows the relative vertical vorticity fields for case G2 at $Ut/a = 6, 9, 12$, and 15. At $Ut/a = 6$, the cyclonic vorticity to the northwest of the mountain range has already developed to a magnitude of 1.0×10^{-4} s^{-1}, compared with 2.5×10^{-4} s^{-1} of the parent cyclone. At $Ut/a = 9$ (Fig. 10b), anticyclonic vorticity develops to the southwest of the mountain range, while the parent cyclone is deflected slightly southward from its original westbound track. At $Ut/a = 12$ (Fig. 10c),

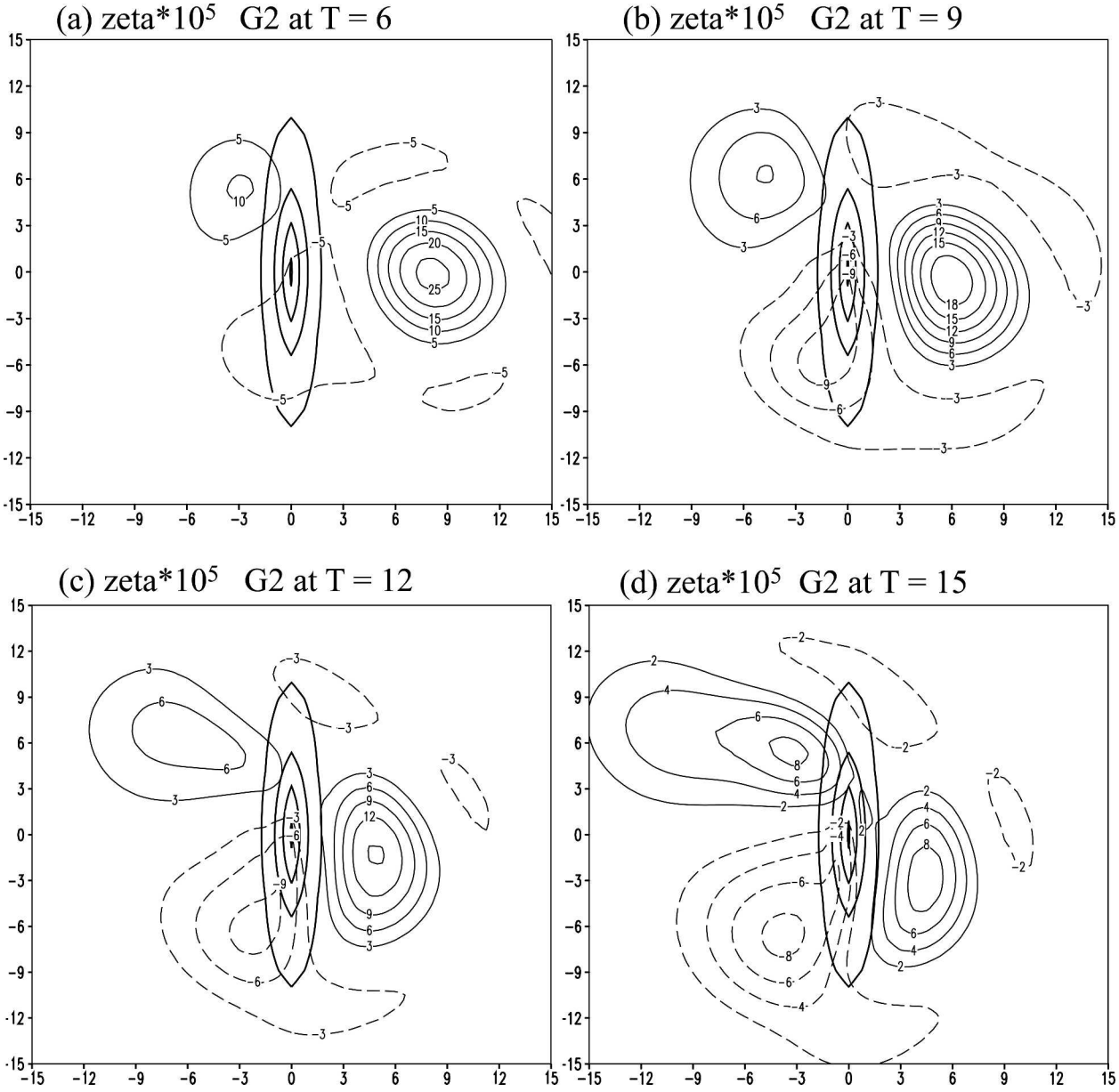

FIG. 10. As in Fig. 7 except for case G2 and with a variable contour interval.

the parent cyclone is deflected farther to the south primarily by vorticity advection (LHHH). The lee vortex expands to a larger area and moves downstream (Figs. 9b and 10c). At $Ut/a = 15$, the lee vortex develops to a strength comparable with the original cyclone vortex, and the lee vortex becomes the main cyclone vortex. Therefore, for a case of strong blocking such as case G2, a cyclone moves more southward along the eastern slope of the mountain range and then appears to "jump" to the northwest slope. The cyclone and flow patterns of case G1 (not shown), with larger R/L_y, are similar to those of G2 but with less southward deflection. This indicates that R/L_y may also serve as a dominant control parameter for cyclone track deflection; a westward-moving cyclone will be deflected more with smaller values of R/L_y. When R/L_y becomes very small, the cyclone will be deflected southward, rather than northward, due to very strong blocking east of the mountain range. The sensitivity of the degree of cyclone track deflection to other nondimensional control parameters, such as h/L_x, U/fL_x, and $V_{\max}/fR$, can be discerned from Table 2. We find that a moving cyclone is deflected more with larger values of h/L_x (mountain steepness) and smaller values of U/fL_x (basic-flow Rossby number), and $V_{\max}/fR$ (nondimensional cyclone vorticity). For example, the degree of cyclone

track deflection decreases for cases A8, F2, C10, and E10 (last row of Fig. 5) as the magnitude of h/L_x decreases from 0.05 to 0.016 (Table 2). The degree of cyclone track deflection decreases for cases A8, A4, and A2 (first column of Fig. 5) as U/fL_x increases from 0.539 to 2.155. The degree of cyclone track deflection is noted to be greater for case A8 ($V_{max}/fR = 1.92$) than for case F6 ($V_{max}/fR = 4.31$).

From these experiments, we found that the track continuity and deflection of a cyclone track are controlled by orographic blocking, which may be represented by other nondimensional control parameters as well as V_{max}/Nh. In other words, the cyclone track becomes discontinuous (continuous) track and the cyclone experiences more (less) deflection when a combination of small (large) values of V_{max}/Nh, U/Nh, R/L_y, U/fL_x, and V_{max}/fR, and large (small) value of h/L_x.

c. Interaction of cyclone circulation with orography and its impacts on the track deflection

An idealized simulation of a cyclone in the vicinity of the idealized mountain range within a quiescent fluid was performed to determine whether orographic blocking is a product of orographic influence on the basic flow or on the outer cyclone circulation. As the outer circulation of a cyclone encounters the mountain range, interactions among the cyclone circulation, basic flow, and the mountain range become very complicated. Orography not only affects the structure and motion of the original vorticity center associated with the parent cyclone, but may contribute to the generation of a new, secondary, vorticity center on the lee side of the mountain range (see Fig. 2). As a new vortex forms on the lee side, the track of the parent cyclone on the windward side may also be influenced by the new vortex. According to Yeh and Elsberry (1993b), an asymmetric circulation may be generated as a mountain barrier significantly changes the inner structure of the cyclone, and ventilation flow (e.g., see their Fig. 15) may then steer the parent cyclone northward. This process is referred to as the ventilation mechanism by Yeh and Elsberry (1993b).

The effects of the interaction between the cyclone circulation and the mountain range in deflecting the cyclone are examined with an idealized experiment (case Q) with no basic flow. Case Q is designed in a manner similar to the control case in LHHH (their Figs. 10 and 11), except with a much larger domain, with $V_{max}/Nh = 0.8$, and without basic flow. Case Q simulates the evolution of a cyclone initially located 200 km to the east ($x/a = 5$) of the idealized CMR within a quiescent fluid.

Figure 11 shows the vorticity fields at $\sigma = 250$ m, for $t = 40 \times 10^3$ s to $t = 320 \times 10^3$ s with a time interval of 40×10^3 s, for case Q. At $t = 40 \times 10^3$ s (Fig. 11a), the center of maximum vorticity has moved slightly to the north following the curvature of the east coast and continues to do so until $t = 160 \times 10^3$ s (Figs. 11b–d). During this time, a secondary vorticity center has developed on the west side of the mountain range. The major vorticity center associated with the parent cyclone is located to the east of the mountain range and expands to encompass a much larger area. Without latent heating and with numerical diffusion and mixing (as described by LHHH), the vorticity of the cyclone decreases in magnitude. At $t = 160 \times 10^3$ s (Fig. 11d), the parent vorticity center continues to weaken, while the secondary vorticity center develops to a strength comparable to that of the upstream vorticity center to the north. By $t = 200 \times 10^3$ s (Fig. 11f), the secondary vorticity center has become the major vorticity center, with two weaker vorticity centers located to the east of the mountain range. At later times in the simulation (Figs. 11g–j), a significant portion of the parent cyclone circulation has already moved over, and to the west side of, the mountain range. Hence, the cyclone vortex appears to jump westward across the mountain range, despite the absence of basic flow to steer the cyclone westward. As seen with cyclones steered by basic flow, the upstream deflection of the drifting cyclone can result from orographic blocking of the outer cyclone circulation.

4. Conclusions and discussion

In this study, we revisited previous studies of TC passage over the Central Mountain Range (CMR) of Taiwan and other significant topography. Using the Buckingham-Π theorem, we identified prospective nondimensional control parameters for cyclone track continuity and deflection in the vicinity of a mesoscale mountain range. These nondimensional control parameters were then examined by performing idealized numerical simulations using a simple numerical model, the NCSU GFD Model.

Based on idealized simulations of a westward-moving cyclone over a north–south oriented mesoscale mountain range, we found that the cyclone track becomes a discontinuous (continuous) track and the cyclone experiences more (less) deflection with a combination of small (large) values of V_{max}/Nh, U/Nh, R/L_y, U/fL_x, and V_{max}/fR, and a large (small) value of h/L_x. Under the situation with discontinuous track, a lee cyclone develops on the lee side of the mountain range and eventually replaces the parent cyclone, as has been observed in reality. Dynamically, this implies that strong (weak) orographic blocking will lead the cyclone track to be discontinuous (continuous). Orographic blocking will result in greater deflection of the moving cyclone to the left or right. In cases featuring very strong blocking, with very small values of V_{max}/Nh, U/Nh, R/L_y, U/fL_x, and V_{max}/fR, and a very large value of h/L_x, a westward-moving cyclone will tend to be deflected southward.

Based on the results of idealized numerical simulations in this study, cyclone track continuity and deflec-

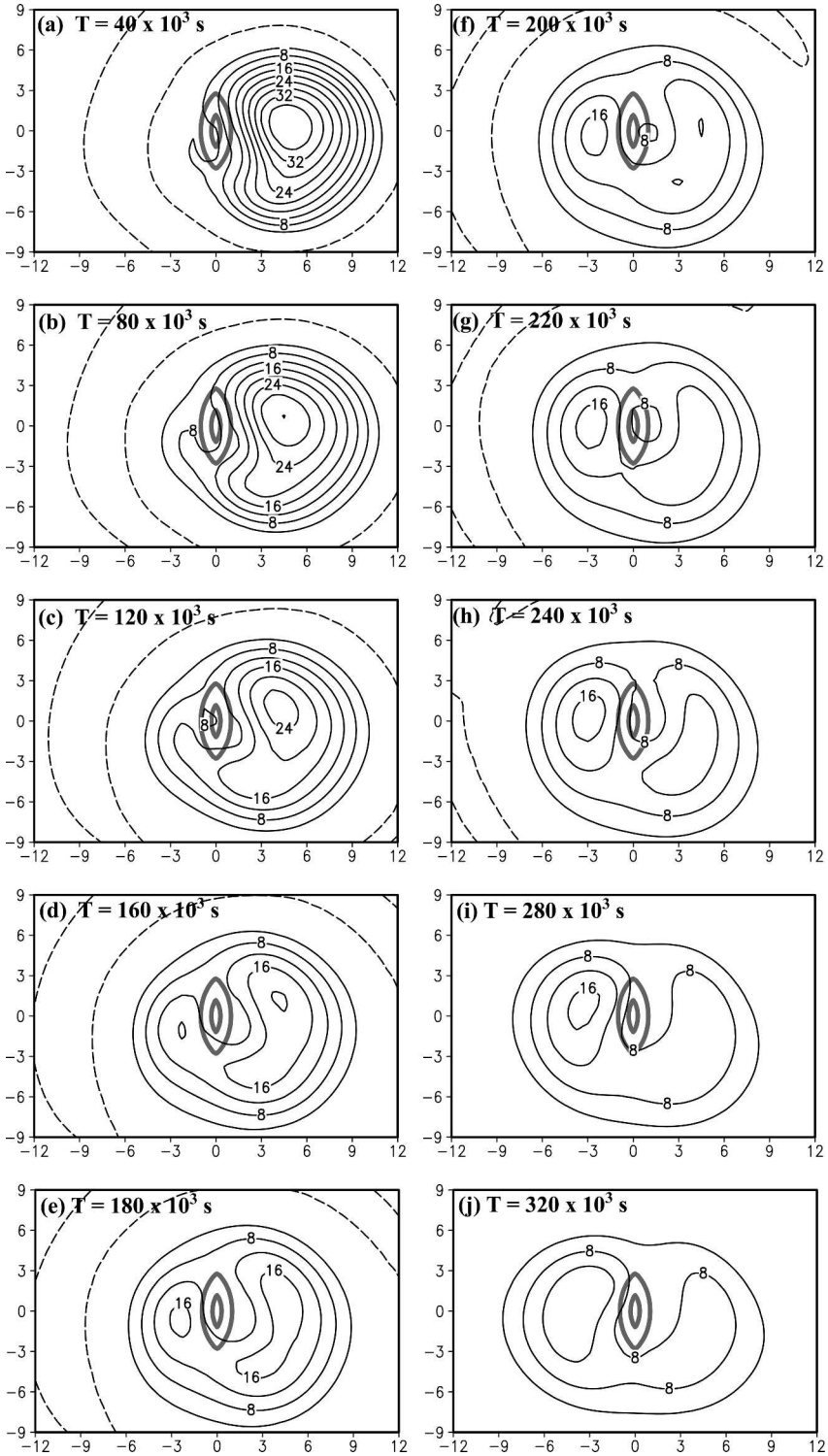

FIG. 11. (Case Q) Vertical relative vorticity fields at $\sigma = 250$ m simulated by NCSU GFD Model of an idealized cyclone originally located to the east of idealized CMR in a quiescent fluid for $t = 40$, 80, 120, 160, 180, 200, 220, 240, 280, and 320×10^3 s. The flow and orographic parameters are $U = 0$ m s^{-1}, $V_{max} = 20$ m s^{-1}, $f = 5.8 \times 10^{-5}$ s^{-1}, $h = 2.5$ km, $a = 40$ km, $b = 120$ km, and $R = 180$ km. The initial cyclone center is located at 200 km ($x/a = 5$) to the east of the mountain peak ($x/a = 0$). The bold lines depict terrain contours of 250 and 1000 m. Vorticity is contoured every 4×10^{-5} s^{-1}.

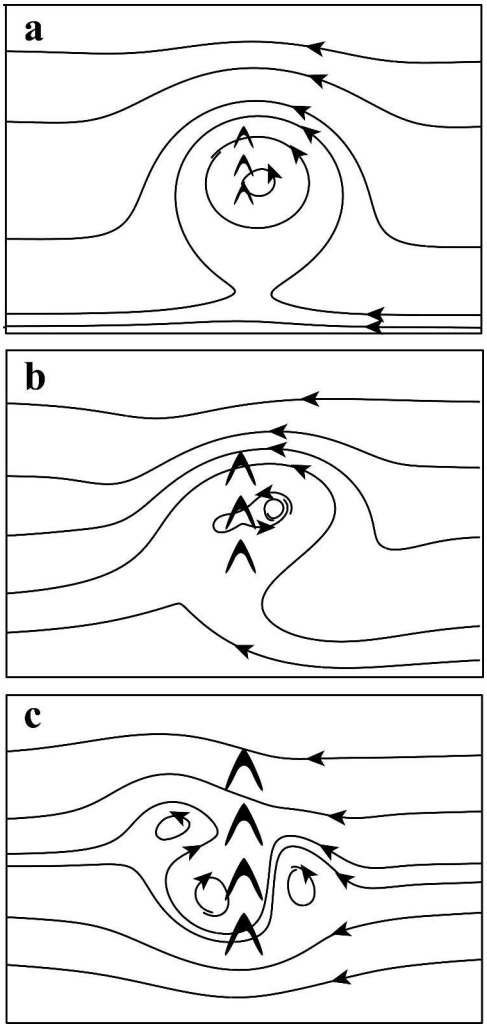

FIG. 12. Conceptual model depicting three different responses of the westward-moving cyclone to orographic forcing. (a) Weak blocking: the cyclone is deflected slightly northward upstream of the mountain range, but follows a continuous track. (b) Moderate blocking: the cyclone is deflected northward upstream of the mountain range, while a secondary vortex forms to the southwest of the mountain range, leading to a discontinuous cyclone track. (c) Strong blocking: the behavior of the cyclone is similar to (b) except the cyclone is deflected to the south and a secondary cyclone is generated at the northwest slope of the mountain range, resulting in a discontinuous track for the cyclone.

tion are summarized in a conceptual model (Fig. 12). With weak orographic blocking (Fig. 12a), a westward-moving cyclone that approaches a mountain range is deflected slightly northward upstream of the mountain and follows a continuous track across the mountain range. With moderate orographic blocking (Fig. 12b), a westward-moving cyclone is deflected northward upstream of a mountain range, while a secondary vortex forms at the southwest slope of the mountain range, resulting in a discontinuous track of the cyclone. When the cyclone scale is comparable to the mountain scale normal to the basic flow, the flow of the outer cyclone circulation is redirected around the northern end of the mountain range. Vorticity is advected northward along the upstream side of the mountain range, and the cyclone is deflected northward. With strong orographic blocking (Fig. 12c), the cyclone is deflected southward and a secondary cyclone forms at the northwest slope of the mountain range, resulting again in a discontinuous track of the cyclone. Due to strong blocking, flow of the cyclone circulation is completely blocked by the mountain range, and a northerly jet is produced between the parent cyclone and the mountain range. This northerly jet then produces strong vorticity advection southward along the upstream side of the mountain range, and effectively deflects the parent cyclone southward.

The experiment with no basic flow was able to isolate the effects of interaction between the outer cyclone circulation and the mountain range in establishing the cyclone track. The cyclone vortex appears to jump westward across the mountain range. With the absence of basic flow, the upstream deflection of the cyclone is explained by orographic blocking of the outer circulation of the cyclone instead of that of the basic flow (e.g., Bender et al. 1987; Schwierz and Davies). Comparing our results with LHHH, the deflection of a moving cyclone can be interpreted as an effect of upstream vorticity advection and leeside vorticity stretching associated with orographic modification of the outer circulation of the cyclone, as opposed to modification of the basic flow as proposed by Chang (1982). Although the mechanism proposed by Carlson (1998) has taken into account the orographic effects on outer circulation of the cyclone, this mechanism cannot explain the cyclonic (rightward) turning of a cyclone crossing the idealized CMR as the horizontal vorticity advection by the outer circulation of the cyclone upstream of the mountain is not taken into account.

A smaller, more realistic westward-moving cyclone approaching the CMR of Taiwan is anticipated to be deflected southward with the presence of strong orographic blocking (Fig. 12c). The northward deflection observed with the majority of TCs approaching the CMR is partially determined by the angle of impingement with the CMR, given that many landfalling TCs have approached the CMR from the southeast. Orographic blocking would then be weaker and the cyclone would pass over the mountain range with some northward deflection.

Control parameters or factors accounting for effects of impinging angles of the basic flow and cyclone circulation, landfall location, latent heating, planetary boundary layer friction, etc., will need to be considered. However, this study provides a systematic approach for understanding the basic dynamics of track continuity and deflection for cyclone moving over a mesoscale mountain range. The findings presented in this study could be applied not only to tropical cyclones, but also

to midlatitude cyclones that encounter mountain ranges in various parts of the world.

Acknowledgments. The authors thank Simon W. Chang, Joseph J. Charney, Hung-Chi Kuo, Ying-Hwa (Bill) Kuo, Shih-Ting Wang, and Chun-Chieh Wu for their valuable discussions. Comments by anonymous reviewers have improved the quality of the manuscript. This study is partially supported by ONR Grant N00014-02-1-0674, NSF Grant ATM-0096876, and UCAR Cooperative Agreement sponsored by NSF ATM-9732665.

REFERENCES

Bender, M. A., R. E. Tuleya, and Y. Kurihara, 1987: A numerical study of the effect of an island terrain on tropical cyclones. *Mon. Wea. Rev.,* **115,** 130–155.

Brand, S., and J. W. Blelloch, 1974: Changes in the characteristics of typhoons crossing the island of Taiwan. *Mon. Wea. Rev.,* **102,** 708–713.

Carlson, T. N., 1998: *Midlatitude Weather Systems*. Amer. Meteor. Soc., 507 pp.

Chang, S. W.-J., 1982: The orographic effects induced by an island mountain range on propagating tropical cyclones. *Mon. Wea. Rev.,* **110,** 1255–1270.

Chiao, S., and Y.-L. Lin, 2003: Numerical simulations of an orographic rainfall event associated with the passage of a tropical storm over a mesoscale mountain. *Wea. Forecasting,* **18,** 325–344.

Han, J., 1998: Large eddy simulations of aircraft wake vortices in a homogeneous atmospheric turbulence. Ph.D. dissertation, North Carolina State University, 162 pp.

Huang, C.-Y., and Y.-L. Lin, 1997: The evolution of a mesoscale vortex impinging on symmetric topography. *Proc. Natl. Sci. Counc. Taiwan Part A,* **21,** 285–309.

Kuo, Y.-H., and W. Wang, 1997: Rainfall prediction of Typhoon Herb with a mesoscale model. Preprints, *Workshop on Typhoon Research in the Taiwan Area*, Boulder, CO, National Science Council (Taiwan), 35–45.

Lin, Y.-L., 1993: Orographic effects on airflow and mesoscale weather systems over Taiwan. *Terr. Atmos. Oceanic Sci.,* **4,** 381–420.

——, N.-H. Lin, and R. P. Weglarz, 1992: Numerical modeling studies of lee mesolows, mesovortices, and mesocyclones with application to the formation of Taiwan mesolows. *Meteor. Atmos. Phys.,* **49,** 43–67.

——, J. Han, D. W. Hamilton, and C.-Y. Huang, 1999: Orographic influence on a drifting cyclone. *J. Atmos. Sci.,* **56,** 534–562.

——, D. B. Ensley, S. Chiao, and C.-Y. Huang, 2002: Orographic influences on rainfall and track deflection associated with the passage of a tropical cyclone. *Mon. Wea. Rev.,* **130,** 2929–2950.

O'Handley, C., and L. F. Bosart, 1996: The impact of the Appalachian Mountains on cyclonic weather systems. Part I: A climatology. *Mon. Wea. Rev.,* **124,** 1353–1373.

Pearson, C. E., Ed., 1983: *Handbook of Applied Mathematics: Selected Results and Methods.* 2d ed. Van Nostrand Reinhold, 1307 pp.

Schwierz, C. B., and H. C. Davies, 2003: Evolution of a synoptic-scale vortex advecting toward a high mountain. *Tellus,* **55A,** 158–172.

Smith, R. B., and A. Gronas, 1993: Stagnation points and bifurcation in 3-D mountain airflow. *Tellus,* **45A,** 28–43.

Smolarkiewicz, P. K., and R. Rotunno, 1989: Low Froude number flow past three-dimensional obstacles. Part I: Baroclinically generated lee vortices. *J. Atmos. Sci.,* **46,** 1154–1164.

Sun, W.-Y., J. D. Chern, C. C. Wu, and W.-R. Hsu, 1991: Numerical simulation of mesoscale circulation in Taiwan and surrounding area. *Mon. Wea. Rev.,* **119,** 2558–2573.

Wang, S.-T., 1980: Prediction of the movement and strength of typhoons in Taiwan and its vicinity. National Science Council Research Rep. 108, Taipei, Taiwan, 100 pp.

Wu, C.-C., and Y.-H. Kuo, 1999: Typhoons affecting Taiwan: Current understanding and future challenges. *Bull. Amer. Meteor. Soc.,* **80,** 67–80.

Yeh, T.-C., and R. L. Elsberry, 1993a: Interaction of typhoons with the Taiwan topography. Part I: Upstream track deflection. *Mon. Wea. Rev.,* **121,** 3193–3212.

——, and ——, 1993b: Interaction of typhoons with the Taiwan topography. Part II: Continuous and discontinuous tracks across the island. *Mon. Wea. Rev.,* **121,** 3213–3233.

Zehnder, J. A., 1993: The influence of large-scale topography on barotropic vortex motion. *J. Atmos. Sci.,* **50,** 2519–2532.

——, and M. J. Reeder, 1997: A numerical study of barotropic vortex motion near a large-scale mountain range with application to the motion of tropical cyclones approaching the Sierra Madre. *Meteor. Atmos. Phys.,* **64,** 1–19.